Ammonia electrosynthesis with a stable metal-free 2D silicon phosphide catalyst

Lv, Chade; Jia, Ning; Qian, Yumin; Wang, Shanpeng; Wang, Xuechun; Yu, Wei; Liu, Chuntai; Pan, Hongge; Zhu, Qiang; Xu, Jianwei; Tao, Xutang; Loh, Kian Ping; Xue, Can; Yan, Qingyu

2023

Lv, C., Jia, N., Qian, Y., Wang, S., Wang, X., Yu, W., Liu, C., Pan, H., Zhu, Q., Xu, J., Tao, X., Loh, K. P., Xue, C. & Yan, Q. (2023). Ammonia electrosynthesis with a stable metal-free 2D silicon phosphide catalyst. Small, 19(10), 2205959-.
https://dx.doi.org/10.1002/smll.202205959

https://hdl.handle.net/10356/166583

https://doi.org/10.1002/smll.202205959

Ammonia electrosynthesis with a stable metal-free two-dimensional phosphorus-based catalyst

Chade Lv[a,h,1], Ning Jia[a,b,1], Yumin Qian[c], Shanpeng Wang[b,*], Wei Yu[d], Chuntai Liu[e], Hongge Pan[f], Qiang Zhu[g], Jianwei Xu[g], Xutang Tao[b], Kian Ping Loh[d], Can Xue[a,*], Qingyu Yan [a,g,*]

[a] School of Materials Science and Engineering, Nanyang Technological University, Singapore, 639798, Singapore
[b] State Key Laboratory of Crystal Materials, Shandong University, Jinan, 250100, China.
[c] Key Laboratory of Advanced Optoelectronic Quantum Architecture and Measurement, Ministry of Education, School of Physics, Beijing Institute of Technology, Beijing 100081, China
[d] Department of Chemistry, National University of Singapore, Singapore 117543, Singapore
[e] Key Laboratory of Materials Processing and Mold Ministry of Education, Zhengzhou University, Zhengzhou 450002, China
[f] Institute of Science and Technology for New Energy, Xi'an Technological University, Xi'an 710021, China
[g] Institute of Materials Research and Engineering, A*STAR, Singapore 138634, Singapore
[h] MIIT Key Laboratory of Critical Materials Technology for New Energy Conversion and Storage, School of Chemistry and Chemical Engineering, Harbin Institute of Technology, Harbin 150001, China

*Corresponding authors.
E-mail addresses: wshp@sdu.edu.cn (S. Wang), cxue@ntu.edu.sg (C. Xue), alexyan@ntu.edu.sg (Q. Yan)
[1] These authors contributed equally to this work.

Ammonia (NH_3) is the indispensable chemical to produce fertilizer for agriculture accompanied with more than 80% of consumption. The large-scale NH_3 production is using the Haber-Bosch process operated at high temperature (400–500 °C) and high pressure (100–200 bar), which necessitates ca. 2% of the global energy and generates ca. 1% of greenhouse gas [1]. Encouraged by demand for sustainability, chemists are seeking alternative and eco-friendly approaches that enable ammonia synthesis under benign conditions. Driven by renewable electricity, NH_3 can be produced from atmospheric N_2 under ambient conditions, namely the electrocatalytic nitrogen reduction reaction (NRR) [2]. Given the merits of such route, it has attracted much attention from the research community to explore advanced NRR electrocatalysts [3].

Very recently, the metal-free two-dimensional (2D) catalysts, such as graphene [4], and polymeric carbon nitride [5], have provided an intriguing picture for high-selectivity electrocatalytic NRR because of their unique surface structure, low cost, high Faradaic efficiency (FE), and relatively slow HER process. Meanwhile, the phosphorus-based materials emerge as standout metal-free 2D catalysts for NH_3 synthesis through N_2 electroreduction. Wang et al. elucidated that the selective NRR process occurred at the active orbital and electrons of zigzag and diff-zigzag type edges on well-exfoliated few-layer black phosphorus nanosheets (FL-BP NSs) through an alternating associative pathway [6]. Nonetheless, the as-exfoliated FL-BP NSs have shown poor chemical stability when exposed to ambient conditions [7], leading to no widespread interest in 2D phosphorus-based catalysts for NRR.

To achieve metal-free two-dimensional phosphorus-based electrocatalysts with high chemical stability, crystalline silicon phosphide nanosheets (C-SiP NSs) were developed by the ultrasonic exfoliation of orthorhombic SiP crystals with weak van der Waals interactions among layers (**Fig. S1** and **S2**), which were prepared based on our previous work (see details in Supplementary materials) [8]. Indicated by the theoretical calculations, the activation of N≡N triple bond can be triggered by the thermodynamically spontaneous adsorption of the N_2 molecule (**Fig. S3**). The N_2-to-NH_3 process could follow an alternating associative pathway with a dimeric end-on N_2 adsorption configuration on the zigzag P sites of C-SiP NSs (see details in Supplementary materials). Suggested by the density functional theory (DFT) calculations, the zigzag P plays a determinant role in converting N_2 into NH_3 (**Fig. S3** and **S4**). Therefore, the C-SiP NSs with sufficient active P atoms may serve as efficient catalysts for electrocatalytic NRR.

X-ray diffraction (XRD) collected on C-SiP NSs indicates strong peaks of (002) and (004) facets of orthorhombic silicon phosphide (ICSD-23724 from Inorganic Crystal Structure Database) with no detectable impurity phase (**Fig. 1a**). X-ray photoelectron spectroscopy (XPS) was conducted to probe the surface chemical status of C-SiP NSs. The Si 2p XPS spectrum can be de-convoluted into the peaks at 98.90 and 100. 45 eV (**Fig. 1b**), which are assignable to the $2p_{1/2}$ and $2p_{3/2}$ signals of Si atoms in orthorhombic SiP [9]. As for the P 2p XPS spectrum shown in **Fig. 1c**, the signals are fitted into the typical $2p_{1/2}$ and $2p_{3/2}$ peaks of SiP [9]. It is noted that the oxidized phosphorus (*i.e.,* PO_x at 133.0~134.0 eV)

peak is absent [10], suggesting good chemical stability of as-obtained C-SiP NSs. The powder was able to stabilize in air for two years without any color change (**Fig. S2**), which generally could not be realized by other phosphorous-based materials, such as black phosphorous. The typical transmission electron microscopy (TEM) image of the obtained C-SiP NSs demonstrates the sheet-like morphology with a decrease size than the bulk SiP (**Fig. 1d**). According the atomic force microscopy (AFM) analysis, the average thickness of C-SiP NSs reaches ~5 nm (**Fig. 1e**). The high-resolution TEM (HRTEM) image displayed in **Fig. 1f** indicates the unambiguous lattice fringes with an interplanar spacing of 3.14 Å, which corresponds to the (130) lattice planes of orthorhombic silicon phosphide. The selected area electron diffraction (SAED) pattern (**Fig. 1g**) shows the diffraction spots of (110), (130) and (150) planes, which suggests as-obtained C-SiP NSs possess good crystallinity. Additionally, these results also disclose that the primary surface of C-SiP NSs is along the (002) facet. From the scanning transmission electron microscopy-energy dispersive spectroscopy (STEM-EDS) analysis of an individual SiP nanosheet (**Fig. 1h**), the Si and P species are uniformly distributed.

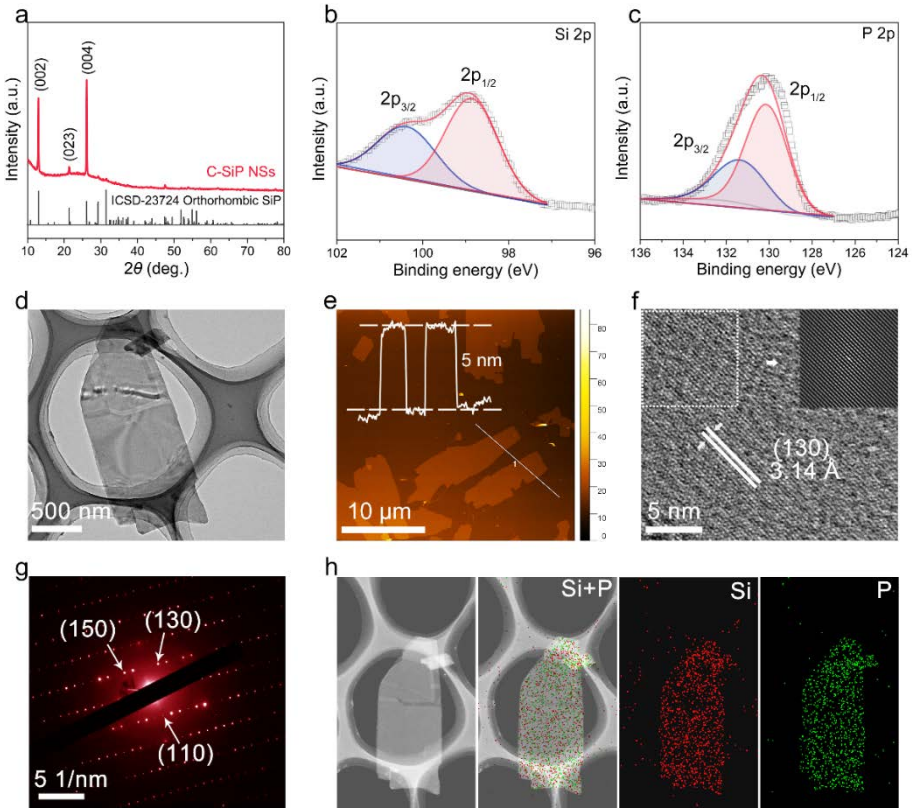

Fig. 1. **Structural characterization of C-SiP NSs.** (a) XRD pattern. (b) Si 2p XPS spectrum. (c) P 2p XPS spectrum. (d) TEM image. (e) AFM image. (f) HRTEM image. (g) SAED pattern. (h) STEM image and corresponding EDS mapping.

To highlight the critical role of the crystalline nature in maintaining the structural stability, we also investigated the amorphous SiP nanosheets (A-SiP NSs), which were obtained using an ultrasonic cell pulverizer with a higher power. Unlike C-SiP NSs with sharp peaks,

the XRD pattern of A-SiP NSs displays no obvious peak (**Fig. S5a**). The Si XPS 2p peaks of A-SiP NSs agrees well with those recorded for C-SiP NSs (**Fig. S5b**). Nevertheless, apart from the peaks for the bulk P anion as illustrated in the P 2p XPS spectrum of A-SiP NSs (**Fig. S5c**), an extra peak emerges at 133.65 eV assignable to the surface oxidized phosphorus [10]. Owing to the surface oxidation, the amorphization results in poor stability of A-SiP NSs, of which the color changes from brown red to white in 3 months. In stark with the regularly-shaped C-SiP NSs, the A-SiP NSs possesses rough edge as shown in the TEM image (**Fig. S5d**). The AFM image displayed in **Fig. S6** not only confirms the irregular edge of A-SiP NSs, but also demonstrates the thickness of ~5 nm. As reflected in the HRTEM image (**Fig. 55e**), there is no lattice fringes for A-SiP NSs because of the amorphous nature. The insert was the corresponding auto-correlation image, which further verified the amorphous structure. The SAED analysis was conducted to affirm the amorphous structure of A-SiP NSs. As displayed in **Fig. S5f**, no diffraction spots or rings but amorphous halo presented in the SAED pattern. The above results verify that the amorphous SiP NSs can be obtained through such high-power ultrasonic approach.

To validate the ammonia synthesis activity over C-SiP NSs under ambient conditions, the electrocatalytic NRR tests were conducted using chrono-amperometry (CA) at fixed potentials in a neutral electrolyte (0.1 M Na_2SO_4) saturated with continuous N_2 bubbling. The ammonia were detected by the indophenol blue method (**Fig. S7**). At the potential of −0.3 V versus RHE, C-SiP NSs reach the maximum NH_3 yield rate of 16.12 μg h^{-1} $mg_{cat.}^{-1}$ (**Fig. 2a**). The corresponding ultraviolet-visible (UV-Vis) spectra and CA curves are displayed in **Fig. 2b** and **Fig. S8**. To evidence the origin of the as-produced NH_3 through the electrocatalytic NRR process on C-SiP NSs, we carried out a series of control tests. With feeding Ar, no NRR activity is delivered by C-SiP NSs under the exact same conditions (**Fig. S9a**). Without loading of C-SiP NSs, only the carbon paper itself can not achieve NH_3 electrosynthesis (**Fig. S9b**). As observed in **Fig. S9c**, the disappearance of NH_3-dependent UV-Vis absorbance peak for test performed at open circuit potential (OCP) indicates that the as-detected ammonia is indeed generated through the electroreduction process. When fed by $^{14}N_2$ for isotopic labeling experiment (**Fig. S10**), a triplet coupling (~ 52 Hz) appears in the ^1H nuclear magnetic resonance (NMR) spectra, which is assignable to the signal of $^{14}NH_4^+$ [11]. In contrast, the employment of $^{15}N_2$ (98 atom % ^{15}N) feeding gas only results in a doublet coupling (~72 Hz), which is indexed to the signal of $^{15}NH_4^+$ [11]. These results can clearly elucidate the N atoms in as-detected NH_3 indeed originate from N_2.

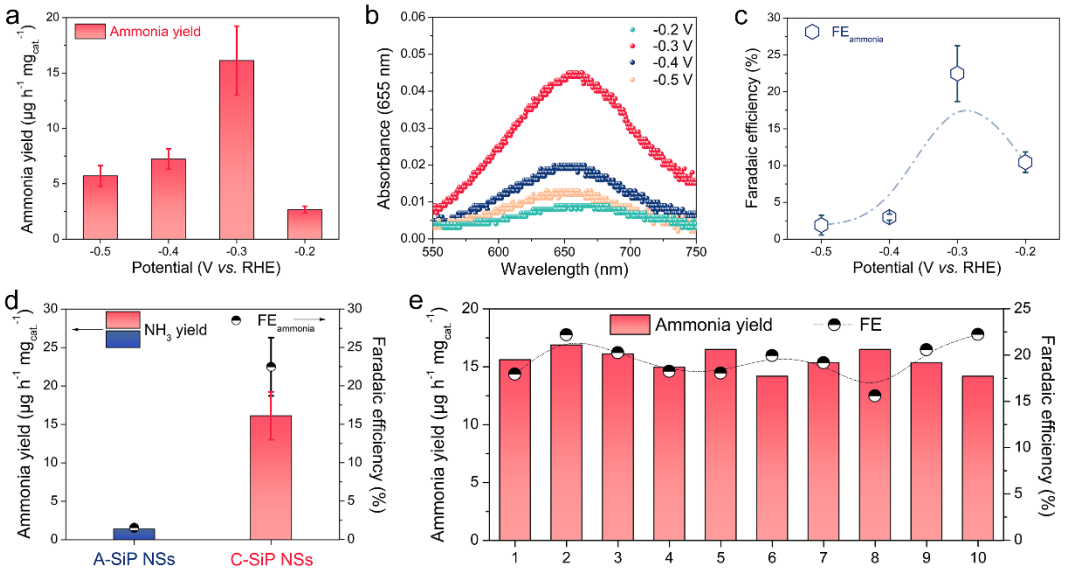

Fig. 2. Electrocatalytic NRR tests for SiP nanosheets at ambient conditions. (a) NH_3 yields. (b) Corresponding UV-Vis spectra. (c) Faradaic efficiencies. (d) NRR performance with different catalysts at −0.3 V versus RHE. (e) 10 runs of recycling tests at −0.3 V versus RHE.

The ammonia production FEs delivered by C-SiP NSs are displayed in the **Fig. 2c**. At −0.3 V versus RHE, C-SiP NSs realize the highest FE of 22.48%. This value exceeds most reported metal-free 2D electrocatalysts as summarized in **Table S1**. To highlight the critical role of surface-active P atoms on C-SiP NSs in N_2 activation and NH_3 production, the electrocatalytic NRR tests were also performed for the surface-oxidized A-SiP NSs. As shown in **Fig. 2d**, A-SiP NSs only deliver an average NH_3 yield rate of 1.40 μg h^{-1} $mg_{cat.}^{-1}$ as well as an extremely low FE of 1.52%. As reflected in the electrochemical double-layer capacitance (C_{dl}) at the solid–liquid interface (**Fig. S11**), the effective surface area of C-SiP NSs is close to that of A-SiP NSs. This excludes the effect of electrochemically active surface area (ECSA) on the difference in NRR performance. Therefore, the sharp decrease in electrocatalytic NRR activity for A-SiP NSs can explicitly confirm the determinant role of crystallinity. The surface stability of C-SiP NSs can lead to stable catalytic performance of the as-developed catalyst, of which the NH_3 yield and FE are basically maintained after ten successive cycles **(Figs. 2e**, **S12** and **S13**). The stability also stands out among many reported metal-free electrocatalysts (**Table S1**). A long-term CA measurement is also performed at −0.3 V versus RHE in 0.1 M Na_2SO_4, and the current density can stabilize for 24 h as observed in **Fig. S14**. Indicated by the XRD patterns (**Fig. S15**), crystalline nature can also be confirmed for C-SiP NSs after electrocatalytic NRR tests. The STEM-EDS mapping suggests the presence of N on the nanosheets after electrocatalytic NRR tests (**Fig. S16**), which affirms the formation of ammonia. As recorded by FTIR spectra for C-SiP NSs after electrocatalytic NRR tests (**Fig. S17**), the $–NH_2$ stretching mode at 1464 cm^{-1} can further prove the ammonia production process on C-SiP NSs electrocatalyst [12].

In summary, the crystalline and amorphous SiP nanosheets were developed through different ultrasonic treatment approaches. However, only the crystalline one can function as a stable metal-free two-dimensional phosphorus-based electrocatalyst for electrocatalytic nitrogen reduction reaction under ambient conditions. As predicted by density functional theory calculation, the zigzag P sites of silicon phosphide allow the favorable activation of N_2 with a dimeric end on adsorption configuration, while the overall NRR process follows the alternating associative pathways. The crystalline nature prevents the SiP nanosheets from surface oxidation, which leads to the maintenance of active P sites. In sharp contrast, the amorphous one loses the surface-active P sites due to the formation of oxidized phosphorus. Thanks to the chemical stability, the crystalline SiP nanosheets realize standout electrocatalytic NRR performance with an NH_3 yield rate of 16.12 μg h^{-1} $mg_{cat.}^{-1}$ and a Faradaic efficiency of 22.48% at −0.3 V versus reversible hydrogen electrode. Hence, we successfully develop a stable metal-free two-dimensional phosphorus-based material and disclose the significant role of surface P sites towards ammonia synthesis, which may provide a mechanistic rationale of electrocatalyst design.

Conflict of interest

The authors declare that they have no conflict of interest.

Acknowledgments

Q.Y. acknowledges the funding support from Singapore MOE AcRF Tier 1 under grant no. 2020-T1-001-031. and Singapore A*STAR project A19D9a0096. C.X. thanks the support from the Ministry of Education Singapore under AcRF-Tier1 (2021-T1-002-012, RG65/21). The authors also like to acknowledge 111 project (D18023) from Zhengzhou University for their support for this work.

Author contributions

Qingyu Yan, Can Xue and Shanpeng Wang conceived the idea and designed the research project. Chade Lv carried out the electrocatalysis tests and most of characterizations. Ning Jia, Shanpeng Wang, and Xutang Tao the samples and conducted the AFM measurments. Yumin Qian carried out the theoretical calculations. Wei Yu and Kian Ping Loh conducted the XPS measurements. Chad Lv, Ning Jia, Chuntai Liu, Hongge Pan, Qiang Zhu, Jianwei Xu, Shanpeng Wang, Can Xue and Qingyu Yan analysed the data. All authors discussed the results and commented on the manuscript.

References

[1] Suryanto BHR, Matuszek K, Choi J, et al. Nitrogen reduction to ammonia at high efficiency and rates based on a phosphonium proton shuttle. Science 2021; 372: 1187-1191.

[2] Garrido-Barros P, Derosa J, Chalkley MJ, et al. Tandem electrocatalytic N_2 fixation via proton-coupled electron transfer. Nature 2022; 609: 71-76.

[3] Liang J, Liu Q, Alshehri AA, et al. Recent advances in nanostructured heterogeneous catalysts for N-cycle electrocatalysis. Nano Res Energy 2022, 1: e9120010.

[4] Yu X, Han P, Wei Z, et al. Boron-doped graphene for electrocatalytic N_2 reduction. Joule 2018; 2: 1610-1622.

[5] Lv C, Qian Y, Yan C, et al. Defect engineering metal-free polymeric carbon nitride electrocatalyst for effective nitrogen fixation under ambient conditions. Angew Chem Int Ed 2018; 57: 10246-10250.

[6] Zhang L, Ding LX, Chen GF, et al. Ammonia synthesis under ambient conditions: selective electroreduction of dinitrogen to ammonia on black phosphorus nanosheets. Angew Chem Int Ed 2019; 58: 2638-2642.

[7] Zhang Y, Wang H, Luo Z, et al. An air-stable densely packed phosphorene-graphene composite toward advanced lithium storage properties. Adv Energy Mater 2016; 6: 1600453.

[8] Li C, Wang S, Li C, et al. Highly sensitive detection of polarized light using a new group IV–V 2D orthorhombic SiP. J Mater Chem C, 2018; 6: 7219-7225.

[9] Li C, Wang S, Zhang X, et al. Controllable seeded flux growth and optoelectronic properties of bulk o-SiP crystals. CrystEngComm 2017; 19: 6986-6991.

[10] Kang J, Wells S A, Wood J D, et al. Stable aqueous dispersions of optically and electronically active phosphorene. Proc Natl Acad Sci USA 2016; 113: 11688-11693.

[11] Andersen S Z, Čolić V, Yang S, et al. A rigorous electrochemical ammonia synthesis protocol with quantitative isotope measurements. Nature 2019; 570: 504-508.

[12] Yao Y, Zhu S, Wang H, et al. A spectroscopic study on the nitrogen electrochemical reduction reaction on gold and platinum surfaces. J Am Chem Soc 2018; 140: 1496-1501.

Graphical abstract: